Steady-state, fluorescence imaging of neoplasia

E.M. Gill, G. Palmer, N. Ramanujam

I. Introduction

Fluorescence imaging has emerged as a promising technique for the early detection of precancer and cancer, a capability that is critical for more effective treatment of this disease, and improved survival rates. Fluorescence imaging is achieved by exciting fluorophores in an area of tissue with specific wavelength(s) of light and measuring the fluorescence response, thus extracting information about the concentration, location, and environment of the fluorophores. The sensitivity and resolution of this technology depends on the ability to establish a source of contrast between the neoplastic and non-neoplastic tissue. This contrast may come from preferential or exclusive presence of the fluorophore within the cancerous tissue, as with exogenous fluorophores, or it may come from more subtle changes in the optical and metabolic characteristics of diseased versus non-diseased tissue, as with endogenous fluorophores. In either case, it is desirable to identify techniques that maximize contrast, and improve resolution and sensitivity; these methods will be further expounded in the following sections.

Once contrast is established, one needs a system capable of imaging this contrast spatially and, if desired, depth-wise. There are a number of approaches to this problem currently being explored, each attempting to ascertain one or both of the two types of information. Spatial information can most directly be acquired using a charge coupled device (CCD) camera to instantaneously image a surface (see for example [1, 2]). In this method, the light can be delivered and collected directly, or coupled through fiber optics. An alternative is to use a single channel photomultiplier tube (PMT) to successively image different points and form an image pixel by pixel, sacrificing speed at a substantial cost savings [3].

Depth imaging is more difficult due to the turbid nature of tissue, but several approaches are being explored. One option is to cut thin sections of tissue and image each transversely (see

for example [4-6]). This method allows one to directly obtain depth information; however, it has the limitation that it requires excision, and so cannot be used diagnostically in vivo. A second approach involves the use of a confocal microscope to extract depth information from tissues in vivo [7]. However the turbid nature of tissue limits the depths that this method can resolve. An alternative approach involves the use of a variable aperture fiber-optic probe. It has been demonstrated using Monte Carlo simulations that the sensitivity to depth depends on the aperture size of the fiber optic probe used to deliver and collect the light from the sample [8]. This approach could have the advantage of reducing the cost and complexity of depth-sensitive in vivo imaging systems, but further experimentation is needed to demonstrate the effectiveness of this method.

Fluorescence imaging of neoplasia has two primary goals. Both of these goals search for a fundamental understanding of the nature of cancer and mechanisms of its growth. Fluorescence imaging can be implemented in animal models to track the progression of the disease [9-12]. This is achieved using molecular reporters such as green fluorescent protein (GFP) [10-12] and luciferase [9, 13-17], that are transfected into the genome of the cancerous cells. The other goal of fluorescence imaging methods is to develop a non-invasive diagnostic tool for human precancer and cancer, that will enable more accurate classification of cancer at an earlier stage than presently available techniques.

In these techniques, the method of exciting the fluorophores can be divided into two categories, single-photon excitation, and two-photon or multi-photon excitation. Single-photon excitation excites each fluorophore with a photon of sufficient energy to elevate it to its excited state. Two-photon excitation, on the other hand, uses lower energy photons (longer wavelength), that are individually incapable of exciting the fluorophore. However, when used at high enough

luminance, two photons can impinge on same fluorophore nearly simultaneously, and their combined energies can promote the fluorophore to its excited state, enabling the emission of a fluorescent photon. This section will focus on single-photon excitation, while the chapter by Peter So will discuss two-photon excitation. We will therefore discuss these methods briefly to distinguish their characteristics and uses.

In two-photon fluorescence imaging, the photons must be focused to a point of intense light in order to have an adequate probability of exciting the fluorophore. This requires that the fluorophore be excited by ballistic photons, whereas in single-photon imaging it is primarily excited by scattered photons [18]. Since the relative number of ballistic photons in turbid media is small, the signal intensity limits the penetration depth relative to single-photon excitation, despite the use of longer wavelengths [19]. Also, the turbidity of tissue requires that high power intensities and signal collection efficiencies be used to deliver and collect sufficient signal, respectively. To achieve this, a high numerical aperture (NA) objective is employed, which at present, renders this method endoscopically incompatible. Two-photon imaging however, has the advantage of exciting fluorophores only in the plane of focus, and is thus inherently suited for optical depth sectioning at high resolution. Unfortunately, the high cost of two-photon imaging components is prohibitive for routine use in clinical applications. Single-photon imaging does not have the image quality or depth sectioning features of two-photon imaging. However, it has a greater penetration depth, is compatible with endoscopic delivery systems and represents a less expensive approach for bulk tissue imaging.

In focusing on the techniques and applications of single-photon fluorescence imaging, three sections will be presented. The first will detail the sources of fluorescence contrast, using both endogenous and exogenous fluorophores. It will also discuss issues related to the scattering

and absorption of light that can make imaging these fluorophores challenging. Second, state of the art instrumentation and imaging strategies will be described in further detail. Finally, the applications of these various techniques will be described. The chapter will be concluded with a section on future prospects of in vivo fluorescence imaging.

II. Tissue Fluorescence Imaging

1. Contrast

Fluorescence imaging requires that there be one or more fluorescent compounds distributed throughout the medium of interest. These may be present intrinsically or they may be introduced artificially by means of injection, ingestion, or genetic manipulation. The relative concentration and distribution of these fluorophores can then be determined using fluorescence imaging techniques (see section III). Localized differences in fluorescence intensities at specific excitation and emission wavelengths provide a means of contrast by which the tissue of interest (e.g. cancer) can be identified. The greater the fluorescence contrast, the more rapidly and accurately these differences can be identified. Therefore it would be desirable to identify those fluorophores, whether endogenous or exogenous, which can maximize contrast.

The amount of contrast is determined by the fluorescence efficiency of the fluorophore of interest, and the concentration and distribution of that fluorophore within the tissue of interest. Endogenous fluorophores have relatively low fluorescence efficiencies, and are typically present in both neoplastic and non-neoplastic tissues. However, neoplasia leads to metabolic and physiologic changes in the tissue, which can alter the properties, concentration and distribution of these fluorophores. For instance, the electron carrier, reduced nictoinamide adenine dinucleotide (NADH) is fluorescent, but its oxidized form is not [20] and therefore this

fluorophore is sensitive to changes in metabolism. The use of endogenous fluorophores has the additional advantage of obviating concerns over the toxicity and mode of application of the fluorophore, as it is already present in the tissue and ready to be imaged. Endogenous fluorophores that may be useful in the diagnosis of neoplasia are shown in Table 1 [21-25, 26, page 15].

Each fluorophore is generally localized to a specific tissue constituent. To illustrate this, fluorescence data from cells and the extracellular matrix (connective tissue) are shown in Figure 1. Specifically, Fig. 1(a,b) shows contour plots of the fluorescence spectra acquired at multiple excitation wavelengths from (a) normal breast (MCF10) cells and (b) collagen I in the extracellular matrix of an organotypic tissue culture. The contour plots shown in Fig. 1 are called fluorescence excitation-emission matrices (EEMs). Each EEM is shown on a log color scale and each contour corresponds to points of equal fluorescence intensity. The meaningful information is straddled by two sets of Rayleigh scattering lines in each EEM. Fig. 1(a) indicates that there are three fluorescence peaks at 280 nm excitation and 340 nm emission (280,340 nm), 340,460 nm, and 450,520 nm. These are attributed to tryptophan, NADH and flavin adenine dinucleotide (FAD) [24]. In Fig. 1(b), the fluorescent peaks at 340, 390 nm can be attributed to the cross-link hydroxyl pyridoline (HP) [21], and that at 280, 340 nm may be attributed to tryptophan [26, page 15].

The second mode of achieving contrast involves artificially introducing fluorophores to the tissue. This can be done by two methods. The first is done by physically introducing fluorophores to the tissue either locally or systemically. The contrast produced by a fluorophore of this type is determined by how well it can preferentially be taken up by the tissue region of interest, as well as the fluorescence properties of the fluorophore itself. The second method

employs genetic manipulation to cause the cells of interest to produce fluorescent or luminescent proteins. This method has an advantage that one can choose to label only the cells of interest (e.g. cancer), and more precisely demarcate the boundaries of the neoplastic tissue. An additional benefit of this method is that it is possible to label specific structures within the cells of interest by encoding these proteins to be attached to an actin molecule [27] for instance, though that is beyond the scope of this chapter. Unfortunately, fluorophores of this type are not suitable for diagnosis in humans, because they require genetic manipulation of cancer cells. Useful exogenous fluorophores are listed in Table 2.

2. Sources of Noise

The concentration and distribution of these fluorophores determine the amount of contrast attainable under optimal conditions. However, tissue is a turbid medium, and therefore, light traveling through it can be scattered and/or absorbed, leading to decreased fluorescence contrast.

Several sources of absorption are present in tissue. In the ultraviolet and visible spectrum, oxy and deoxy-hemoglobin are the dominant absorbers [28]. Absorption decreases in the near infrared (NIR) [28]. However this is outside the range in which intrinsic fluorophores are excitable, so tissue imaging at these wavelengths requires an extrinsic source of fluorescence. These effects are highly wavelength dependent and result in an attenuation of the excitation and emission light traveling through the tissue. This limits the penetration depth of light and therefore, the depth of imaging.

Another difficulty in deep tissue imaging is scattering. This occurs due to inhomogeneities in the index of refraction of the tissue, arising from membranes and other tissue

structures. This causes blurring of the signal and limits the depth and size of regions from which localized fluorescence can be detected [29].

Each of the previous sources of difficulty in fluorescence imaging deal with getting light to and from the fluorophore of interest, but it is also possible for the fluorophore itself to exhibit different properties as a result of interactions with other fluorophores or its environment. One important interaction to consider in tissue imaging is photobleaching. This occurs for both intrinsic and extrinsic fluorophores in a manner and rate that is specific to each individual molecule. For example, fluorescein has been shown to photobleach faster at higher concentrations due to fluorescein-fluorescein interactions [30], whereas the rate of photobleaching of protoporphyrin IX (PpIX), the fluorophore produced from δ-amino levulinic acid (5-ALA), has been shown to be predominantly oxygen and irradiance dependent [31].

III. Instrumentation and Imaging Strategies

Single-photon fluorescence imaging can in principle yield spatial and depth-wise information. Furthermore, at each pixel and/or voxel, fluorescence intensity can be measured at different wavelengths to provide spectral information, and time resolved fluorescence decay can be measured to provide the excited state lifetime of the molecules. Ultimately these techniques can merge in order to exploit as much information as possible from fluorescence imaging. In the following sections, fluorescence imaging strategies and the information content of these techniques are outlined for in vitro and in vivo applications. Additionally, advances in techniques for depth-resolved fluorescence imaging in vivo are discussed.

1. In Vitro Imaging Strategies

In order to explore the relationship between tissue fluorescence and the presence of dysplasia, a method is needed that can establish the source and distribution of fluorescence contrast within tissue. This is difficult to do in vivo because bulk tissue is optically thick, or turbid. Therefore, in vitro techniques employing optically thin tissue slices/sections represent a logical means for obtaining this information. When choosing a method it is important to consider whether the in vitro model realistically represents the in vivo environment. This is particularly important for characterizing endogenous fluorophores that are involved in biochemical processes. For example, fluorescence from fluorophores such as NADH and FAD yields information about the reduction-oxidation (redox) state of tissue metabolism [20]. If the metabolic and/or oxygenation state of the tissue is altered in vitro, the measurement will be affected; therefore preserving the metabolic state of in vitro samples or keeping the samples viable in some way is important for fluorescence studies.

1.a Fluorescence microscopy of unstained, frozen tissue sections

Conventionally, unstained frozen tissue sections are cut and then imaged at room temperature using fluorescence microscopy. The tissue oxidizes at room temperature, which can affect the metabolic state and hence the fluorescence characteristics of the tissue sample.

Although this method is not ideal, results from studies that examine differences between normal and dysplastic tissue, have been able to set a qualitative precedent for in vivo studies. Fluorescence microscopy of fluorescent tissue micro-structures has been performed on unstained, frozen sections of a variety of tissue types, including the cervix [32], skin [33], breast

[34], lung [35], aero-digestive tract [36], brain [37] and colon [4, 38-42]. Romer et al. [38] observed an increase in the fluorescence intensity of dysplastic epithelial cells relative to that of normal cells, when they were excited at 350-360 nm. Fiarman et al. [39] also observed an increase in the dysplastic cell fluorescence intensity at 488 nm excitation. Furthermore, Bottiroli et al. [41] observed a red fluorescence at around 630 nm when some parts of neoplastic tissue sections were excited at 366 nm, which was attributed to porphyrins. Romer et al. [38] and Fiarman et al. [39] observed a decreased fluorescence intensity from the collagen in the lamina propria of the adenomatous colon, relative to that of the normal colon at 350-360 nm and 488 nm excitation, respectively. The results of these investigations, which were performed on unstained, frozen tissue sections, support the use of fluorescence imaging to distinguish between optically thick, neoplastic and non-neoplastic tissues, in vivo.

1.b Fluorescence microscopy of short-term tissue cultures

The use of short-term tissue cultures instead of unstained, frozen tissue sections provides a way to avoid problems associated with oxidation by maintaining the tissue's viability in vitro [5, 6].

Brookner et al. [5] introduced a novel sample preparation technique that seeks to maintain the viability and metabolic status of biopsied cervical tissue. They prepared short-term tissue cultures from ~200 μm thin slices of cervical biopsies, and imaged autofluorescence using fluorescence microscopy. Spatial patterns of fluorescence imaged from the transverse samples were strongly correlated with patient age. Addition of potassium cyanide (which impedes oxidative phosphorylation and alters the redox state of the tissue) produced increased fluorescence in the basal and superficial layers of the epithelium, which was attributed to NADH.

These results validate the sample preparation method, which provides a preferable alternative to imaging unstained, frozen tissue sections at room temperature. Caveats of this technique are that the thin tissue slices are fragile and difficult to prepare, and must be imaged within a time window of 5 hours or less post-biopsy. Also, variations in the tissue-slice thickness (+/- 10%) make quantitative comparisons of fluorescence intensity difficult.

Drezek et al. [6] employed the same sample preparation technique to examine differences in the autofluorescence of normal and dysplastic cervical tissue. An increase in epithelial fluorescence intensity at 380 nm excitation was observed in dysplastic relative to normal tissue. This change was tentatively assigned to a change in concentration of NADH. A decrease in the stromal fluorescence intensity at 380 nm and 460 nm excitation was observed in dysplastic relative to normal tissue, which was assigned to a decrease in collagen concentration. Interestingly, these results suggest that stromal fluorescence is influenced by the presence of dysplasia in the epithelium before stromal invasion occurs. One possible reason for this is increased levels of metalloproteinases that break down the extracellular matrix. This important observation gives evidence that the tissue microenvironment surrounding precancer exhibits biochemical changes that can be detected with fluorescence.

1.c Low-temperature fluorescence imaging of freeze-trapped tissue blocks

Low-temperature fluorescence imaging involves milling a flat surface of frozen tissue sections and consequently imaging the fluorescence, while the tissue is in the frozen state. The frozen tissue contains the intact vasculature and the metabolic state is preserved [24]. One caveat is that fluorescence intensities at low temperatures (-196 °C) do not directly represent the

fluorescence intensities of in vivo tissue (at 37 °C). However relative comparisons are indicative of in vivo changes.

A low temperature fluorometer has been designed (constructed at the Johnson Foundation of the University of Pennsylvania) [43], which is uniquely suited for imaging the fluorescence of freeze-trapped tissue blocks at liquid nitrogen temperatures. A schematic of the mechanical part of the apparatus is shown in Figure 2. The sample is embedded in isopentane or other tissue-freezing medium and placed in the liquid nitrogen chamber. The instrument incorporates a milling head that creates a flat imaging surface on the frozen tissue and provides the ability to sequentially image planar sections that can be combined to form a 3-D image. The optical scanner consists of a mercury arc lamp, PMT, and excitation and emission filter wheels. Light is transmitted to and detected from the sample via a micro-light-guide. The distal end of the light guide is precisely positioned at a fixed distance above the imaging surface, typically at a distance of 50 μm. The scanning stage contains a stepper motor which steps the light guide across the imaging surface in discrete steps. Fluorescence intensities are recorded from each discrete pixel on the tissue surface at several excitation-emission wavelength pairs.

Ramanujam et al. [44] have used this instrument to image the autofluorescence from freeze-trapped cervical biopsy cross-sections. Figure 3 illustrates fluorescence images from a normal cervical biopsy at excitation-emission wavelength pairs of 440, 525 nm and 365, 460 nm, and the corresponding histological hemotoxylin and eosin (H&E) stained white light image. At 440, 525 nm the fluorescence is primarily attributed to FAD while fluorescence at 365, 460 nm is attributed to NADH [24]. An increase in the color intensity scale corresponds to an increase in the fluorescence intensity. These images indicate that fluorescence intensity at 440, 525 nm is localized in the stromal section while fluorescence intensity at 365, 460 nm is more prevalent in

the epithelial layer (see H&E stain for orientation). Figure 4 displays the average fluorescence intensity as a function of tissue depth at (a) 440, 525 nm and (b) 365, 460 nm for a normal, inflammatory and severely dysplastic tissue. Evaluation of Figure 4(a) indicates that the intensity at 440, 525 nm is significantly greater in the stroma relative to that in the epithelium for all three tissue types. Figure 4(b) indicates no significant difference in intensity with depth for tissues with inflammation and severe dysplasia; however it does indicate a difference in intensity with depth for normal tissue.

1.d Tissue culture models

Long-lived tissue culture models could provide a nearly ideal, 3-D in vivo model for imaging tissue fluorescence and in particular, changes in fluorescence with dysplasia. One such organotypic culture model has been developed at the University of Wisconsin Medical School and consists of a collagen base plated with the Near-diploid Immortalized Keratinocyte Skin (NIKS) human cell line [45]. It has been shown that a fully stratified squamous epithelium is formed, which includes the basal cell layer and an underlying extracellular matrix. Applications for this system are far-reaching and include its potential use in transplants for burn victims and in high throughput schemes for applications such as drug-discovery. With regard to dysplasia, this system is nearly ideal, because cancer proliferation can be studied in a human tissue culture system without the need for animal models. Cancerous cells such as squamous cell carcinoma (SCC) cells, with and without GFP, can be added to the basal layer to simulate neoplastic disease progression in the epithelium. Additionally, changes in the tissue microenvironment with dysplasia can be studied. Furthermore, 3-D fluorescence imaging with depth-sectioning can

potentially be performed with confocal and/or multi-photon fluorescence imaging techniques. One caveat of this system is the exclusion of a blood supply.

1.e Summary

The strategies described above provide the basis for in vivo imaging, by shedding light on the distribution of fluorescence contrast in tissue. Most of these methods have been used to look at endogenous fluorescence contrast. They can also be extended to examine exogenous tissue fluorescence contrast. These studies also establish the importance of measuring depth-wise fluorescence to gain an additional dimension of information [6, 44].

2. In Vivo Imaging Strategies

As mentioned above, one of the challenges imposed upon in vivo fluorescence imaging is tissue turbidity, or the influence of absorption and scattering on the fluorescence signal. Another challenge is to resolve fluorescence from heterogeneous and depth-dependent sources. In this section we examine instrumentation currently used for in vivo fluorescence imaging and review the different imaging strategies associated with these instruments.

The various types of instruments employed for in vivo fluorescence imaging essentially have the same basic components, except for a few differences. For a thorough description of the characteristics of individual components, the reader is referred to [28]. A schematic of the basic components of such an instrument is shown in Figure 5. It consists of either a broadband or monochromatic excitation light source, a dispersing element or filter to spectrally select the excitation band, a delivery and collection conduit for the delivery of excitation light to, and the collection of the emitted light from the imaging surface of the biological medium, a dispersing

element or filter to spectrally select the emitted light, and a multi- or single-channel detector, which measures the spatial and/or spectral distribution of the intensity of the emitted light. Typical systems employ multi-channel detectors; however, it is possible in principle to raster-scan a narrow excitation beam over a surface area and collect the emitted light with a single-channel detector [3].

2.a Multi-channel endoscopic and nonendoscopic methods

Several groups have developed endoscopic-compatible [2, 46-58] and nonendoscopic-based [59-64] fluorescence imaging systems. One system originally developed by Palcic et al. [46] for fluorescence bronchoscopy, has led to a commercial light-induced fluorescence endoscopy (LIFE) device (Xillix Technologies Corporation, Richmond, BC, Canada) that is used for fluorescence imaging of relatively large tissue fields (a few centimeters in diameter).

Anderssson-Engels et al. [60] describe a nonendoscopic multispectral imaging system for differentiating neoplastic and non-neoplastic tissue. This system uses a pulsed nitrogen laser with 4 ns pulses at an excitation wavelength of 337 nm. The excitation is directed via a dichroic mirror to illuminate a tissue surface area of 10 mm x 10 mm. The fluorescence emitted from the tissue is transmitted through the same dichroic mirror at wavelengths above 370 nm and impinges on a Cassegrainian telescope. This telescope consists of a set of four different bandpass filters, a primary mirror split in four segments, and an output mirror. Each part of the primary mirror is tilted slightly off the optical axis producing four separate images of the same area of tissue in the plane of the imaging detector. Each image occupies one quadrant of the detector and corresponds to one of the four spectral colors. In this manner, the images corresponding to the four spectral channels are recorded simultaneously. An aperture is used in

front of the first telescope mirror to improve image resolution. The detection system consists of a dual microchannel plate image-intensified and Peltier cooled (5 ^{o}C) CCD camera. The image intensifier is gated at 200 ns to integrate the fluorescent light while suppressing the ambient light. The spatial resolution of the instrument was determined to be 0.5 mm. In this study, the filters were chosen based on the spectral characteristics of tissue autofluorescence as well as the photosensitizer, Photofrin.

In a later study, the multispectral imaging system was modified for use with the photosensitizer δ-amino levulinic acid (5-ALA) [61]. Modifications included the addition of a dye laser which emits at 405 nm with a pulse duration of 3 ns, an increased imaging area of 25 mm x 35 mm, different bandpass filters, a shorter 100 ns gating time, and further cooling of the CCD camera to –30 ^{o}C. In both studies, the four images were arithmetically combined to produce maximum contrast between the tumor and surrounding normal skin.

Wang et al. [1, 2] describe a colonoscope, modified for autofluorescence imaging of colonic neoplasms. Specifically, they incorporate a fiber optic excitation probe into a videocolonoscope that is able to perform conventional colonoscopy as well as fluorescence imaging, in an in vivo setting. The modified endoscopic-based imaging system consists of a high-powered Argon laser, producing excitation at 356 nm, and an intensified charge injection device (CID) camera. The image is transmitted through a spatially coherent optical fiber bundle and is spectrally filtered with a 400-nm long-pass filter prior to detection. Table 3 lists parameters for this multi-channel imaging system. Autofluorescence images are collected with an excitation wavelength of 356 nm and emission in the spectral band of 400-700 nm.

2.b Single channel methods: The Flying Spot Scanner

As mentioned earlier, it is in principle possible to perform fluorescence imaging with a single-channel detector provided the imaging area is raster scanned. Such an instrument has been developed, the details of which are described.

The Flying Spot Scanner (FSS) [3], constructed at the University of Pennsylvania consists of three primary components as shown in Figure 6. A 442 nm wavelength, Helium-Cadmium laser is the light source. A mechanical positioning assembly directs the excitation light from the laser to the tissue and directs the emitted light from the tissue though a filter wheel into a PMT, which is contained within the mechanical positioning assembly. The assembly also provides three degrees of freedom for illumination and collection: tilt, rotation and translation. Between the laser and the assembly is a box, which contains the electronic and optical components for deflection of the laser illumination in the horizontal and vertical directions, electronics for signal detection and processing, and a computer interface.

The laser light passes through a chopper, two scanning mirrors and a series of plano convex lenses and flat mirrors, before it is incident on the tissue surface. The excitation light is scanned across the tissue surface and the emitted light from each discrete pixel is collected and focused by a Fresnel lens onto the PMT. Between the Fresnel lens and the PMT is a filter wheel that contains four filters. These filters are chosen to selectively transmit fluorescence while rejecting back-scattered excitation light, and also for reflectance measurements. A neutral density filter is used in a second filter wheel slot to ensure that the fluorescence and reflectance signals are within the same dynamic range. The FSS accounts for ambient light conditions and the dark current through a simple real-time subtraction scheme. Table 3 lists the parameters of the single-channel system.

Figure 7 illustrates an image recorded with the FSS: (a) Autofluorescence and reflectance ratio (F/R) images and (b) normalized F/R profiles of a 9L glioma tumor (9 days) and adjacent muscle tissue in the rat flank are shown.

2.c Signal to noise comparison of multi-channel and single-channel methods

The FSS represents a significant decrease in cost, relative to multi-channel, fluorescence-imaging systems. The reduction in cost would result from the use of relatively low-power light sources and single-channel detectors. However, it is important to confirm that the less-expensive FSS performs comparably to the multi-channel systems. To address this issue, the performance of the FSS was compared to that of the multi-channel fluorescence-imaging system developed by Wang et al. [1] for the detection of pre-cancers in the colon (described in section 2.a). The characteristics of the two systems are shown in Table 3. The multi-channel system illuminates a 40 mm diameter area with a power density of 0.239 mW/mm^2. If the illumination area is reduced to 10 mm in diameter, the power density is increased to 4 mW/mm^2, which is within a factor of two reported for the FSS. A reduction in the working distance by a factor of two doubles the spatial resolution of the FSS, making both the working distance and spatial resolution of the single-channel system comparable to that of the multi-channel system. The signal-to-noise ratios (SNR) of the two systems are also very similar. However, the frame rate of the multi-channel system is 30 times faster compared to that of the FSS. Thus, it can be concluded that the FSS will represent a low-cost alternative to multi-channel fluorescence imaging-systems in applications where high frame rates are not required.

2.d Summary

These strategies represent the range of in vivo fluorescence imaging techniques in existence. Endoscopic instruments are convenient for in vivo use, while non-endoscopic methods are more appropriate for imaging large surface areas. The FSS illustrates the potential for imaging large tissue areas with good image quality and low cost, which is important in the development of clinical diagnostic tools. In all of these methods the excitation light probes an unknown volume of tissue, which contains as yet, unresolved depth-dependent information.

3. In Vivo Imaging Strategies for Imaging depth-wise Fluorescence

The imaging strategies described above integrate over tissue depth, which loses the depth distribution of fluorescence. Drezek and Ramanujam's in vitro work [6, 44] suggests that depth-wise information, especially in the case of endogenous fluorescence may provide additional contrast in fluorescence imaging.

The next challenge for in vivo fluorescence imaging is to develop a technique for measuring depth-wise fluorescence. A primary consideration is the illumination and collection geometry. Diffuse reflectance and fluorescence emitted from the tissue surface is non-isotropic due to the filtering effect of absorption and scattering. It can be hypothesized that the probed volume depends on the aperture of the source.

3.a Confocal microscopic methods

Confocal microscopy is the only conventional technique extended to obtaining 3-D fluorescence images of turbid media. The method employs a high NA objective to create a focal plane of light that can be scanned within a limited distance along the z-axis. Sophisticated

instruments are able to image fluorescence in real-time and have been used for such applications as observing calcium signaling in cardiac muscle [65].

Several groups have applied confocal microscopy to fluorescence imaging of tissue, in vivo and in vitro [7, 66-68]. Sabharwal and Rouse et al. [7, 68] have developed a confocal microendoscope for in vivo imaging and further adapted it for multispectral imaging. They measured the performance by imaging fluorescent microspheres, and cultured and stained live cells, stained prostate tissue, and the stained peritoneum of a live mouse [7]. This system consists of an argon-ion laser, illumination and detection optics, a CCD camera, and a fiber optic imaging bundle that incorporates a miniature objective lens and focusing mechanism. The overall diameter of the fiber bundle is 1 mm with an active image diameter of 720 μm. The focusing mechanism allows imaging to a depth of 200 μm below the tissue surface. The instrument exhibits a lateral resolution of 3 μm and a depth resolution of 25 μm. Using a slit instead of point aperture makes imaging faster. For a more detailed description of the apparatus the reader is referred to [7]. To collect spectral information, a prism is added to the detection arm that disperses the emitted light onto the CCD camera. In this configuration, the spectral resolution is 11 nm; however, the spectral resolution can change with prism geometry or with the substitution of a diffraction grating. Spectral information can be processed to isolate emission bands and to provide image reconstruction that enhances contrast or provides specific information about the tissue.

In general, confocal microscopic techniques are limited by the highly scattering nature of tissue, yielding a low signal-to-noise ratio in the absence of strong contrast. Moreover, the depth from which the fluorescence is detected using confocal methods is superficial; that is, the detected volume is on the scale of the mean free scattering path [66], which is typically about

100 μm in the UV-VIS [69-71]. Furthermore, this approach requires the use of high-powered light sources and sensitive detectors, which can make the cost of this technology prohibitive for routine cancer screening and diagnosis. It is therefore important to develop an alternate strategy that can image the depth dependent distribution of a fluorescent target in a turbid medium with an improved signal-to-noise ratio, increased penetration depth and reduced cost.

3.b Variable aperture methods

A possible alternative to 3-D imaging with confocal microscopy may be obtained with a particular fiber optic probe geometry and illumination-collection scheme. Results from Monte Carlo modeling of fluorescent emission from a homogeneous tissue indicate that there is an approximately linear relationship between the optical fiber diameter and the probed depth within the tissue [72]. As has been discussed earlier, the emitted fluorescence itself has a geometric dependence due to the filtering effects of tissue scattering and absorption [69]. An optical fiber probe illumination-collection scheme that yields fluorescence measurements that are independent of this geometric dependence consists of a geometry in which the emitted light from the tissue is collected only from that surface directly illuminated by the excitation light [73]. Consequently, it has been suggested that it is possible to measure the depth-wise distribution of fluorescence using an optical fiber probe with a variable aperture and a coincident illumination and detection light path [8].

Quan et al. [8] have performed Monte Carlo simulations to model the fluorescence from cancerous tissue (SCC) and cancerous tissue tagged with the molecular marker green fluorescent protein (SCC-GFP). The tissue optical properties and fluorescence efficiencies that served as input to the Monte Carlo simulation were estimated from reports in the literature. The

fluorescence was calculated as a function of probe aperture diameter and for varying fluorescent target depths and the results are illustrated in Figures 8 and 9. Figure 8 displays the normalized fluorescence ratio versus aperture diameter for the model containing: (a) the SCC layer (without GFP) and (b) the SCC-GFP layer. Each curve represents the ratio of two profiles: the fluorescence detected for a model containing the SCC layer and that detected for a model without the SCC layer (equivalent to a normal epithelium). The legend displays the depth and thickness of the SCC layer for each profile. Figure 9 displays the aperture diameter that corresponds to the minimum (for SCC) and maximum (for SCC-GFP) normalized fluorescence ratio (MFR) versus the depth of the SCC layer. A fit to the data indicates that there is a linear relationship between the MFR diameter and depth over the range of 50-300 μm, which implies that the MFR correlates with the depth of the fluorescent target. The next step is to experimentally test the theoretical model with turbid samples of increasing complexity until it can ultimately be tested in vivo.

3c. Other suggested methods

It has been suggested [6] that an algorithmic approach for elucidation of depth-wise fluorescence is possible. However, there are no analytical algorithms such as the Diffusion approximation [74, 75] that describe light propagation through tissue, that are valid in the ultraviolet/visible regions where tissue absorption and scattering are similar in magnitude. It is feasible that the Diffusion approximation will find use in applications that use exogenous fluorophores that emit at wavelengths in the far red and near infrared.

Another approach is to use variable wavelengths to resolve depth-wise information. However, while it is true that the penetration depth of light in turbid media depends on the

wavelength, this approach is inherently confounded by other variables that also have spectral dependencies.

IV. Applications

1. Autofluorescence imaging

The goal of imaging autofluorescence in tissue is to be able to accurately and noninvasively diagnose human neoplasia. Table 1 lists endogenous fluorophores that may be useful in the diagnosis of neoplasia and their properties. These endogenous fluorophores, described earlier in this chapter, generally exhibit weak fluorescence, thus requiring sensitive detection techniques to distinguish differences between dysplastic and normal tissue. The presence of multiple fluorophores with broad and overlapping spectral characteristics makes the choice of the most diagnostically relevant wavelengths nontrivial. For this reason, the sophistication of imaging schemes has evolved over time. Imaging strategies began simply, using a single excitation-emission wavelength pair and today use several excitation-emission wavelength pairs or spectral bands of fluorescence in addition to diffuse reflectance and white light images [54, 76, 77]. The multiple fluorescence images provide complementary information to each other, and to the other imaging modalities. Typically they are arithmetically combined to maximize image contrast or to provide specific information, such as the tissue metabolic state in redox ratio imaging [20, 44].

Table 3 lists recent articles on autofluorescence imaging of neoplasia in a wide variety of organ sites. The reader is referred to the individual references for details on these applications.

2. Photosensitizer Imaging

The use of photosensitive materials for fluorescence imaging of tissue grew from their use in photodynamic therapy (PDT), an emerging therapeutic technique for treatment of atherosclerosis and dysplasia. Mature lesions take up certain photosensitive agents preferentially with respect to surrounding normal tissue and can be targeted with destructive, high intensity light. Reasons for the preferential uptake are not fully understood; however, one mechanism that may play a role is the extravasation [78] that occurs in the vasculature of the lesion.

An advantage of using exogenous fluorophores is that the photophysical and pharmocokinetic properties can be selected and are known. Furthermore, exogenous fluorophores are more highly fluorescent than endogenous fluorophores. On the other hand, the disadvantage of using exogenous fluorophores is that issues relating to safety and toxicity of the drug being used have to be addressed. Also, the selection of the optimal time delay after administration of the drug is non-trivial. Furthermore, there is no specificity to the biochemical aspects of disease process itself.

Table 2 lists exogenous fluorophores used for imaging neoplasia in tissue. Their spectral characteristics and selected applications are listed as well.

3. Molecular Imaging

A very exciting and newly emerging field examines cellular- and molecular-specific probes for fluorescence imaging applications. With this approach, the disease of interest can potentially be studied in detail as well as precisely localized within tissue. The high specificity of these techniques provides opportunities to target cellular and molecular changes in the tissue microenvironment with neoplasia, such as in the metastatic process. By these means it may be possible to understand disease mechanisms and accelerate development of therapeutic strategies.

In this section we describe current molecular fluorescence imaging techniques, the potential of which have yet to be fully exploited.

Optical reporter genes are transgenes that consist of a luminescent or fluorescent molecule that has been bound to an expressed gene or promoter. Tumor cells may be genetically manipulated to express optical reporter genes. Yang et al. have developed tumor cells that express green fluorescent protein (GFP) and have used these cells to monitor tumor growth and metastases in nude mice [10-12]. Fluorescent tumors have also been used to provide contrast for monitoring angiogenesis [12]. The non-luminous capillaries are visible against the bright tumor fluorescence and blood vessel density is quantitatively measured either with intravital or whole body imaging. In these studies, the fluorescent probe is introduced to the live animal model in different ways. The GFP-expressing tumor cells are orthotopically implanted, intravenously injected, or adenoviral GFP is directly injected into the major organs.

Whole body imaging is achieved with a fluorescent light box and an intensified and/or cooled CCD camera. Alternatively, trans-illuminated or epifluorescence microscopy is an option. With whole body imaging of fluorescence from GFP, a 60 μm tumor is detectable at a depth of 0.5 mm, and an 1800 μm tumor is detectable at 2.2 mm below the surface [10]. Figure 10(a,c,d) illustrates whole body images of liver and skull metastases in a mouse model, imaged with a fluorescent light box and cooled CCD camera [10]. The lesions were formed by orthotopically transplanting GFP-labeled tumor cells to live nude mice. The cross-sectional image shown in Fig. 10(b) was acquired using conventional fluorescence microscopy.

A technique called bioluminescence imaging (BLI) uses the optical reporter firefly luciferase, bound to viral promoters to tag tumor cells [9, 13-16, 79]. Detection of luciferase-labeled cells is extremely sensitive and can detect as few as 1000 human tumor cells distributed

throughout the peritoneal cavity of a mouse [9, 15]. This means that the full disease course may be monitored including very early cancer. Edinger et al. [15] have developed a stable HeLa cell line that expresses the modified firefly luciferase gene. In a recent study by Rehemtulla et al. [16], BLI was established as a quantitative tool for assessment of antineoplastic therapies. Quantification of cell kill as a result of chemotherapy was performed with BLI and magnetic resonance imaging (MRI) with comparable results.

The use of optical reporter genes for fluorescence imaging of neoplasia provides an extremely useful tool for understanding the mechanisms of disease and in particular the interaction between neoplastic cells and the surrounding microenvironment. This technique allows the use of live animal models where regulatory processes and pathways of gene expression are intact. As this research area matures, the predictability of animal models of human disease will improve since study groups can be followed over time. This exciting technique lends itself well to taking advantage of GFP mutants that emit in the NIR where the optical transmission through tissue is relatively high.

Another exciting technique is immunofluorescence imaging. In this case, imaging is achieved by binding fluorophores to antibody molecules that interact with specific antigens, delivering the fluorophore to the specific site of interest [80]. The fluorophore persists on the time scale of days making it possible to monitor the effect of therapeutic interventions such as radiation therapy and chemotherapy. This technique also has high specificity and does not require the use of potentially toxic compounds. In vivo immunofluorescence studies are limited by the rate of antibody delivery to the binding site, which is in part determined by the molecular weight of the antibody, typically 150 kDa. For more details on this technique the reader is referred to the excellent chapter by Ramjiawan [80].

V. Future Prospects

Near infrared (NIR) absorption and diffuse reflectance spectroscopy are well-established techniques for imaging tissue due to the spectral advantage of being within an optical window where the absorption is low compared to scattering. Analytical theories such as the Diffusion approximation to the transport equation approximate light propagation in this spectral region fairly accurately [74, 75]. Major applications of these techniques target perfusion and vascularization, and are not related to the fluorescence characteristics of neoplastic tissue; however, there are some instances of NIR imaging of photosensitizers and molecular reporters in tissue.

The fluorescent dye, indocyanine green (ICG) has been used for liver biopsy [81] while the photosensitizer, lutetium texaphyrin has been used for PDT of cancers and atheromatous plaque [82-85]. New cyanine dyes structurally related to ICG, have been synthesized for use as contrast agents for biomedical optical imaging [86]. These dyes exhibit enhanced quantum yield, are faster acting and last longer relative to ICG. This work demonstrates the potential for engineering dyes to optimize fluorescence imaging in the near infrared.

NIR molecular reporters are used in tumor labeling [87]. Becker et al. have developed a peptide-dye conjugate consisting of cyanine dye and the somatostatin analog octreotate. This approach combines the specificity of ligand/recepor interaction with NIR fluorescence detection. Immunofluorescence imaging has also been performed using cyanine-labeled antibodies [88-91].

A new cell-permeant probe, DRAQ5 has been developed for cytometric analysis of the cell cycle and provides 3-D nuclear structure and location in live and fixed cells with

fluorescence microscopic techniques [92]. New probes to image tumor-associated protease activity can detect early stage tumors in vivo [93, 94].

VI. References

1. **Wang, T.D., *et al.*, *Mathematical model of fluorescence endoscopic image formation.* Applied Optics, 1998. 37(34): p. 8103-8111.**
2. **Wang, T.D., *et al.*, *In vivo identification of colonic dysplasia using fluorescence endoscopic imaging.* Gastrointest Endosc, 1999. 49(4 Pt 1): p. 447-55.**
3. **Ramanujam, N., *et al.*, *Fast and noninvasive, fluorescence imaging of biological tissues, in vivo using a flying-spot scanner.* IEEE Transactions on Biomedical Engineering, 2001. 48(9).**
4. **Wang, H.W., *et al.*, *Quantitative laser scanning confocal autofluorescence microscopy of normal, premalignant, and malignant colonic tissues.* IEEE Trans Biomed Eng, 1999. 46(10): p. 1246-52.**
5. **Brookner, C.K., *et al.*, *Autofluorescence patterns in short-term cultures of normal cervical tissue.* Photochem Photobiol, 2000. 71(6): p. 730-6.**
6. **Drezek, R., *et al.*, *Autofluorescence microscopy of fresh cervical-tissue sections reveals alterations in tissue biochemistry with dysplasia.* Photochem Photobiol, 2001. 73(6): p. 636-41.**
7. **Sabharwal, Y.S., *et al.*, *Slit-scanning confocal microendoscope for high-resolution in vivo imaging.* Applied-Optics, 1999. 38(34): p. 7133-44.**
8. **Quan, L. and N. Ramanujam, *Correlation between the depth of a fluorescent target in a turbid medium and the illumination-collection aperture diameter.* submitted, Optics Letters, 2001.**
9. **Contag, C.H., *et al.*, *Use of reporter genes for optical measurements of neoplastic disease in vivo.* Neoplasia, 2000. 2(1-2): p. 41-52.**
10. **Yang, M., *et al.*, *Whole-body optical imaging of green fluorescent protein-expressing tumors and metastases.* Proc Natl Acad Sci U S A, 2000. 97(3): p. 1206-11.**
11. **Yang, M., *et al.*, *Visualizing gene expression by whole-body fluorescence imaging.* Proc Natl Acad Sci U S A, 2000. 97(22): p. 12278-82.**
12. **Yang, M., *et al.*, *Whole-body and intravital optical imaging of angiogenesis in orthotopically implanted tumors.* Proc Natl Acad Sci U S A, 2001. 98(5): p. 2616-2621.**
13. **Contag, C.H., *et al.*, *Visualizing gene expression in living mammals using a bioluminescent reporter.* Photochem Photobiol, 1997. 66(4): p. 523-31.**
14. **Contag, P.R., *et al.*, *Bioluminescent indicators in living mammals.* Nat Med, 1998. 4(2): p. 245-7.**
15. **Edinger, M., *et al.*, *Noninvasive assessment of tumor cell proliferation in animal models.* Neoplasia, 1999. 1(4): p. 303-10.**
16. **Rehemtulla, A., *et al.*, *Rapid and quantitative assessment of cancer treatment response using in vivo bioluminescence imaging.* Neoplasia, 2000. 2(6): p. 491-5.**
17. **Tamulevicius, P. and C. Streffer, *Metabolic imaging in tumours by means of bioluminescence.* Br J Cancer, 1995. 72(5): p. 1102-12.**

18. **Gan, X. and M. Gu, *Fluorescence microscopic imaging through tissue-like turbid media.* J Applied Physics, 2000. 87(7): p. 3214-21.**
19. **Min, G., *et al.*, *Comparison of penetration depth between two-photon excitation and single-photon excitation in imaging through turbid tissue media.* Applied Physics Letters, 2000. 77(10): p. 1551-3.**
20. **Masters, B.R. and B. Chance, *Redox Confocal Imaging: Intrinsic Fluorescent Probes of Cellular Metabolism*, . p. 44-57.**
21. **Fujimoto, D., *The Structure of Pyridinoline, a Collagen Crosslink.* Biochem. Biophys. Res. Commun., 1977. 76(4): p. 1124-1129.**
22. **Deyl, Z., *et al.*, *Studies on the chemical nature of elastin fluorescence.* Biochim Biophys Acta, 1980. 625(2): p. 248-54.**
23. **Thornhill, D.P., *Separation of a series of chromophores and fluorophores present in elastin.* Biochem J, 1975. 147(2): p. 215-9.**
24. **Chance, B., *et al.*, *Oxidation-reduction ratio studies of mitochondria in freeze-trapped samples. NADH and flavoprotein fluorescence signals.* J Biol Chem, 1979. 254(11): p. 4764-71.**
25. **Kluftinger, A.M., *et al.*, *Detection of squamous cell cancer and pre-cancerous lesions by imaging of tissue autofluorescence in the hamster cheek pouch model.* Surg Oncol, 1992. 1(2): p. 183-8.**
26. **Lakowicz, J.R., *Principles of fluorescence spectroscopy*. 2nd ed. 1999, New York: Kluwer Academic/Plenum. xxiii, 698.**
27. **Pawlak, G. and D.M. Helfman, *Cytoskeletal changes in cell transformation and tumorigenesis.* Curr Opin Genet Dev, 2001. 11(1): p. 41-7.**
28. **Ramanujam, N., *Fluorescence Spectroscopy In Vivo*, in *Encyclopedia of Analytical Chemistry*, R.A. Meyers, Editor. 2000, John Wiley & Sons Ltd. p. 20-56.**
29. **Xingde, L., B. Chance, and A.G. Yodh, *Fluorescent heterogeneities in turbid media: limits for detection, characterization, and comparison with absorption.* Applied-Optics, 1998. 37(28): p. 6833-44.**
30. **Song, L., *et al.*, *Influence of fluorochrome labeling density on the photobleaching kinetics of fluorescein in microscopy.* Cytometry, 1997. 27(3): p. 213-23.**
31. **Finlay, J.C., *et al.*, *Porphyrin bleaching and PDT-induced spectral changes are irradiance dependent in ALA-sensitized normal rat skin in vivo.* Photochem Photobiol, 2001. 73(1): p. 54-63.**
32. **Lohmann, W., *et al.*, *Native fluorescence of unstained cryo-sections of the cervix uteri compared with histological observations.* Naturwissenschaften, 1989. 76(3): p. 125-7.**
33. **Lohmann, W. and E. Paul, *Native fluorescence of unstained cryo-sections of the skin with melanomas and nevi.* Naturwissenschaften, 1989. 76(9): p. 424-6.**
34. **Lohmann, W. and S. Kunzel, *Fluorescence tomographical studies on breast tissue with cancer.* Naturwissenschaften, 1990. 77(10): p. 476-8.**
35. **Lohmann, W., *et al.*, *Fluorescence studies on lung tumors.* Z Naturforsch [C], 1990. 45(9-10): p. 1063-6.**
36. **Fryen, A., *et al.*, *Significance of autofluorescence for the optical demarcation of field cancerisation in the upper aerodigestive tract.* Acta Otolaryngol, 1997. 117(2): p. 316-9.**
37. **Bottiroli, G., *et al.*, *Brain tissue autofluorescence: an aid for intraoperative delineation of tumor resection margins.* Cancer Detect Prev, 1998. 22(4): p. 330-9.**

38. **Romer, T.J., *et al.*, *Laser-induced fluorescence microscopy of normal colon and dysplasia in colonic adenomas: implications for spectroscopic diagnosis.* Am J Gastroenterol, 1995. 90(1): p. 81-7.**
39. **Fiarman, G.S., *et al.*, *Differences in laser-induced autofluorescence between adenomatous and hyperplastic polyps and normal colonic mucosa by confocal microscopy.* Dig Dis Sci, 1995. 40(6): p. 1261-8.**
40. **Izuishi, K., *et al.*, *The histological basis of detection of adenoma and cancer in the colon by autofluorescence endoscopic imaging.* Endoscopy, 1999. 31(7): p. 511-6.**
41. **Bottiroli, G., *et al.*, *Natural fluorescence of normal and neoplastic human colon: a comprehensive "ex vivo" study.* Lasers Surg Med, 1995. 16(1): p. 48-60.**
42. **DaCosta, R.S., *et al.*, *Confocal Microscopy/macroscopy and microspectrofluorimetry analysis of human colorectal tissue.* J. Anal Morphol, 1997. 4: p. 192-194.**
43. **Quistorff, B., J.C. Haselgrove, and B. Chance, *High spatial resolution readout of 3-D metabolic organ structure: an automated, low-temperature redox ratio-scanning instrument.* Anal Biochem, 1985. 148(2): p. 389-400.**
44. **Ramanujam, N., *et al.*, *Low temperature fluorescence imaging of freeze-trapped human cervical tissues.* Optics-Express., 2001. 8(6).**
45. **Allen-Hoffmann, B.L., *et al.*, *Normal growth and differentiation in a spontaneously immortalized near- diploid human keratinocyte cell line, NIKS.* J Invest Dermatol, 2000. 114(3): p. 444-55.**
46. **Palcic, B., *et al.*, *Detection and localization of early lung cancer by imaging techniques.* Chest, 1991. 99(3): p. 742-3.**
47. **DuVall, G.A. and J. Kost, *Laser Induced Fluorescence Endoscopy (LIFE): a Pilot Study of a Real Time Autofluorescence Imaging System for Early Detection of Dysplasia and Carcinoma in the GI Tract.* Endoscopy, 1996. 28(S45).**
48. **Zargi, M., *et al.*, *Laser induced fluorescence in diagnostics of laryngeal cancer.* Acta Otolaryngol Suppl, 1997. 527: p. 125-7.**
49. **Wagnieres, G.A., A.P. Studzinski, and H.E. van den Bergh, *An endoscopic fluorescence imaging system for simultaneous visual examination and photodetection of cancers.* Review-of-Scientific-Instruments, 1997. 68(1, pt.1): p. 203-12.**
50. **DuVall, G.A., B.C. Wilson, and N. Marcon, *Tissue Autofluorescence.* Ann. Gastrointest. Endosc., 1997. 10: p. 25-30.**
51. **Lam, S., *et al.*, *Localization of bronchial intraepithelial neoplastic lesions by fluorescence bronchoscopy.* Chest, 1998. 113(3): p. 696-702.**
52. **Kulapaditharom, B. and V. Boonkitticharoen, *Laser-induced fluorescence imaging in localization of head and neck cancers.* Ann Otol Rhinol Laryngol, 1998. 107(3): p. 241-6.**
53. **McKechnie, T., *et al.*, *An endoscopic system for the early detection of cancers of the gastrointestinal tract.* Review-of-Scientific-Instruments, 1998. 69(6): p. 2521-3.**
54. **Svanberg, K., *et al.*, *Clinical multi-colour fluorescence imaging of malignant tumours-- initial experience.* Acta Radiol, 1998. 39(1): p. 2-9.**
55. **Zeng, H., *et al.*, *Real-time endoscopic fluorescence imaging for early cancer detection in the gastrointestinal tract.* Bioimaging, 1998. 6(4): p. 151-65.**
56. **Izuishi, K., *et al.*, *Detection of bile duct cancer by autofluorescence cholangioscopy: a pilot study.* Hepatogastroenterology, 1999. 46(26): p. 804-7.**

57. **Betz, C.S., *et al.*, *Autofluorescence imaging and spectroscopy of normal and malignant mucosa in patients with head and neck cancer.* Lasers Surg Med, 1999. 25(4): p. 323-34.**

58. **Haringsma, J., *et al.*, *Autofluorescence endoscopy: feasibility of detection of GI neoplasms unapparent to white light endoscopy with an evolving technology.* Gastrointest Endosc, 2001. 53(6): p. 642-50.**

59. **Andersson, P.S., S. Montan, and S. Svanberg, *Multispectral system for medical fluorescence imaging.* IEEE-Journal-of-Quantum-Electronics, 1987. QE-23(10): p. 1798-805.**

60. **Andersson Engels, S., J. Johansson, and S. Svanberg, *Medical diagnostic system based on simultaneous multispectral fluorescence imaging.* Applied-Optics, 1994. 33(34): p. 8022-9.**

61. **Andersson Engels, S., *et al.*, *Multi-colour fluorescence imaging in connection with photodynamic therapy of delta -amino levulinic acid (ALA) sensitised skin malignancies.* Bioimaging, 1995. 3(3): p. 134-43.**

62. **Chwirot, B.W., *et al.*, *Detection of melanomas by digital imaging of spectrally resolved ultraviolet light-induced autofluorescence of human skin.* Eur J Cancer, 1998. 34(11): p. 1730-4.**

63. **Hewett, J., *et al.*, *The application of a compact multispectral imaging system with integrated excitation source to in vivo monitoring of fluorescence during topical photodynamic therapy of superficial skin cancers.* Photochem Photobiol, 2001. 73(3): p. 278-82.**

64. **Qu, J.Y., H. Zhijian, and H. Jianwen, *Mapping the fluorescence yield on turbid media.* Applied-Physics-Letters, 2000. 76(8): p. 970-2.**

65. **Blatter, L.A. and E. Niggli, *Confocal near-membrane detection of calcium in cardiac myocytes.* Cell Calcium, 1998. 23(5): p. 269-79.**

66. **Pogue, B.W. and T. Hasan, *Fluorophore quantitation in tissue-simulating media with confocal detection.* IEEE-Journal-of-Selected-Topics-in-Quantum-Electronics, 1996. 2(4): p. 959-64.**

67. **Pogue, B.W. and G. Burke, *Fiber-optic bundle design for quantitative fluorescence measurement from tissue.* Applied-Optics, 1998. 37(31): p. 7429-36.**

68. **Rouse, A.R. and A.F. Gmitro, *Multispectral imaging with a confocal microendoscope.* Optics-Letters, 2000. 25(23): p. 1708-10.**

69. **Welch, A.J., *et al.*, *Propagation of fluorescent light.* Lasers Surg Med, 1997. 21(2): p. 166-78.**

70. **Zeng, H., *et al.*, *Spectroscopic and microscopic characteristics of human skin autofluorescence emission.* Photochem Photobiol, 1995. 61(6): p. 639-45.**

71. **Zonios, G.I., *et al.*, *Morphological model of human colon tissue fluorescence.* IEEE Trans Biomed Eng, 1996. 43(2): p. 113-22.**

72. **Pfefer, T.J., *et al.*, *Light propagation in tissue during fluorescence spectroscopy with single fiber probes.* submitted, IEEE J Sel Top Quant Electron, 2001.**

73. **Richards-Kortum, R., *et al.*, *Spectral diagnosis of atherosclerosis using an optical fiber laser catheter.* Am Heart J, 1989. 118(2): p. 381-91.**

74. **Furutsu, K., *Diffusion equation derived from space-time transport equation.* Journal of the Optical Society of America, 1980. 70(4): p. 360-6.**

75. **Kim, A.D. and A. Ishimaru, *Optical diffusion of continuous-wave, pulsed, and density waves in scattering media and comparisons with radiative transfer.* Applied Optics, 1998. 37(22): p. 5313-19.**

76. **Andersson-Engels, S., *et al.*, *In vivo fluorescence imaging for tissue diagnostics.* Phys Med Biol, 1997. 42(5): p. 815-24.**

77. **Qu, J.Y., Z. Huang, and H. Jianwen, *Excitation-and-collection geometry insensitive fluorescence imaging of tissue-simulating turbid media.* Applied-Optics, 2000. 39(19): p. 3344-56.**

78. **Ito, S., *et al.*, *Real-time observation of micrometastasis formation in the living mouse liver using a green fluorescent protein gene-tagged rat tongue carcinoma cell line.* Int J Cancer, 2001. 93(2): p. 212-7.**

79. **Xenogen Corporation, A.A., Alameda, California 94501, USA, .**

80. **Ramjiawan, B., M. Jackson, and H. Mantsch, *Fluorescence Imaging*, in *Encyclopedia of Analytical Chemistry*. 2000.**

81. **Kimura, Y., *et al.*, *Usefulness of indocyanine green injection during ultrasound-guided liver biopsy for the diagnosis of small hepatocellular carcinoma.* Acta Med Okayama, 1996. 50(5): p. 255-9.**

82. **Woodburn, K.W., *et al.*, *Phototherapy of cancer and atheromatous plaque with texaphyrins.* J Clin Laser Med Surg, 1996. 14(5): p. 343-8.**

83. **Woodburn, K.W., *et al.*, *Localization and efficacy analysis of the phototherapeutic lutetium texaphyrin (PCI-0123) in the murine EMT6 sarcoma model.* Photochem Photobiol, 1997. 65(3): p. 410-5.**

84. **Young, S.W., *et al.*, *Lutetium texaphyrin (PCI-0123): a near-infrared, water-soluble photosensitizer.* Photochem Photobiol, 1996. 63(6): p. 892-7.**

85. **Zellweger, M., *et al.*, *Fluorescence pharmacokinetics of Lutetium Texaphyrin (PCI-0123, Lu-Tex) in the skin and in healthy and tumoral hamster cheek-pouch mucosa.* J Photochem Photobiol B, 2000. 55(1): p. 56-62.**

86. **Licha, K., *et al.*, *Hydrophilic cyanine dyes as contrast agents for near-infrared tumor imaging: synthesis, photophysical properties and spectroscopic in vivo characterization.* Photochem Photobiol, 2000. 72(3): p. 392-8.**

87. **Becker, A., *et al.*, *Receptor-targeted optical imaging of tumors with near-infrared fluorescent ligands.* Nat Biotechnol, 2001. 19(4): p. 327-31.**

88. **Ballou, B., *et al.*, *Tumor labeling in vivo using cyanine-conjugated monoclonal antibodies.* Cancer Immunol Immunother, 1995. 41(4): p. 257-63.**

89. **Ballou, B., *et al.*, *Tumor detection and visualization using cyanine fluorochrome-labeled antibodies.* Biotechnol Prog, 1997. 13(5): p. 649-58.**

90. **Folli, S., *et al.*, *Antibody-indocyanin conjugates for immunophotodetection of human squamous cell carcinoma in nude mice.* Cancer Res, 1994. 54(10): p. 2643-9.**

91. **Ramjiawan, B., *et al.*, *Noninvasive localization of tumors by immunofluorescence imaging using a single chain Fv fragment of a human monoclonal antibody with broad cancer specificity.* Cancer, 2000. 89(5): p. 1134-44.**

92. **Smith, P.J., *et al.*, *Characteristics of a novel deep red/infrared fluorescent cell-permeant DNA probe, DRAQ5, in intact human cells analyzed by flow cytometry, confocal and multiphoton microscopy.* Cytometry, 2000. 40(4): p. 280-91.**

93. **Tung, C.H., *et al.*, *In vivo imaging of proteolytic enzyme activity using a novel molecular reporter.* Cancer Res, 2000. 60(17): p. 4953-8.**

94. **Weissleder, R., *et al.*, *In vivo imaging of tumors with protease-activated near-infrared fluorescent probes.* Nat Biotechnol, 1999. 17(4): p. 375-8.**

95. **Mayinger, B., *et al.*, *Endoscopic photodynamic diagnosis: oral aminolevulinic acid is a marker of GI cancer and dysplastic lesions.* Gastrointest Endosc, 1999. 50(2): p. 242-6.**

96. **Leunig, A., *et al.*, *Fluorescence imaging and spectroscopy of 5-aminolevulinic acid induced protoporphyrin IX for the detection of neoplastic lesions in the oral cavity.* Am J Surg, 1996. 172(6): p. 674-7.**

97. **Leunig, A., *et al.*, *Detection of squamous cell carcinoma of the oral cavity by imaging 5- aminolevulinic acid-induced protoporphyrin IX fluorescence.* Laryngoscope, 2000. 110(1): p. 78-83.**

98. **Leunig, A., *et al.*, *Fluorescence staining of oral cancer using a topical application of 5-aminolevulinic acid: fluorescence microscopic studies.* J Photochem Photobiol B, 2001. 60(1): p. 44-9.**

99. **Lange, N., *et al.*, *Photodetection of early human bladder cancer based on the fluorescence of 5-aminolaevulinic acid hexylester-induced protoporphyrin IX: a pilot study.* Br J Cancer, 1999. 80(1-2): p. 185-93.**

100. **Nauta, J.M., *et al.*, *In vivo photo-detection of chemically induced premalignant lesions and squamous cell carcinoma of the rat palatal mucosa.* J Photochem Photobiol B, 1997. 39(2): p. 156-66.**

101. **Stummer, W., *et al.*, *Intraoperative detection of malignant gliomas by 5-aminolevulinic acid- induced porphyrin fluorescence.* Neurosurgery, 1998. 42(3): p. 518-25; discussion 525-6.**

102. **Tatman, D., *et al.*, *Carotenohematoporphyrins as tumor-imaging dyes. Synthesis and in vitro photophysical characterization.* Photochem Photobiol, 1998. 68(4): p. 459-66.**

103. **Kajiyama, N. and E. Nakano, *Isolation and characterization of mutants of firefly luciferase which produce different colors of light.* Protein Eng, 1991. 4(6): p. 691-3.**

104. **Viviani, V.R. and Y. Ohmiya, *Bioluminescence color determinants of Phrixothrix railroad-worm luciferases: chimeric luciferases, site-directed mutagenesis of Arg 215 and guanidine effect.* Photochem Photobiol, 2000. 72(2): p. 267-71.**

105. **Cubitt, A.B., *et al.*, *Understanding, improving and using green fluorescent proteins.* Trends Biochem Sci, 1995. 20(11): p. 448-55.**

106. **Wiehler, J., J. von Hummel, and B. Steipe, *Mutants of Discosoma red fluorescent protein with a GFP-like chromophore.* FEBS Lett, 2001. 487(3): p. 384-9.**

107. **Yang, T.T., *et al.*, *Improved fluorescence and dual color detection with enhanced blue and green variants of the green fluorescent protein.* J Biol Chem, 1998. 273(14): p. 8212-6.**

108. **Tsien, R.Y., *The green fluorescent protein.* Annu Rev Biochem, 1998. 67: p. 509-44.**

109. **Ito, Y., M. Suzuki, and Y. Husimi, *A novel mutant of green fluorescent protein with enhanced sensitivity for microanalysis at 488 nm excitation.* Biochem Biophys Res Commun, 1999. 264(2): p. 556-60.**

110. **Chishima, T., *et al.*, *Visualization of the metastatic process by green fluorescent protein expression.* Anticancer Res, 1997. 17(4A): p. 2377-84.**

111. **Becker, A., *et al.*, *Macromolecular contrast agents for optical imaging of tumors: comparison of indotricarbocyanine-labeled human serum albumin and transferrin.* Photochem Photobiol, 2000. 72(2): p. 234-41.**

112. **Blumenkranz, M.S., *et al.*, *Lutetium texaphyrin (Lu-Tex): a potential new agent for ocular fundus angiography and photodynamic therapy.* Am J Ophthalmol, 2000. 129(3): p. 353-62.**

113. **Bornhop, D.J., *et al.*, *Fluorescent tissue site-selective lanthanide chelate, Tb-PCTMB for enhanced imaging of cancer.* Anal Chem, 1999. 71(14): p. 2607-15.**

114. **Hubbard, D.S., *et al.*, *Endoscopic fluorescence imaging of tissue selective lanthanide chelates.* Bioimaging, 1998. 6(2): p. 63-70.**

115. **Nikas, D.C., J.W. Foley, and P.M. Black, *Fluorescent imaging in a glioma model in vivo.* Lasers Surg Med, 2001. 29(1): p. 11-7.**

116. **van Staveren, H.J., *et al.*, *Fluorescence imaging and spectroscopy of ethyl nile blue A in animal models of (pre)malignancies.* Photochem Photobiol, 2001. 73(1): p. 32-8.**

117. **Cubeddu, R., *et al.*, *Fluorescence imaging during photodynamic therapy of experimental tumors in mice sensitized with disulfonated aluminum phthalocyanine.* Photochem Photobiol, 2000. 72(5): p. 690-5.**

118. **Witjes, M.J., *et al.*, *Distribution of aluminum phthalocyanine disulfonate in an oral squamous cell carcinoma model. In vivo fluorescence imaging compared with ex vivo analytical methods.* Photochem Photobiol, 1997. 65(4): p. 685-93.**

119. **Zellweger, M., *et al.*, *Stability of the fluorescence measurement of Foscan in the normal human oral cavity as an indicator of its content in early cancers of the esophagus and the bronchi.* Photochem Photobiol, 1999. 69(5): p. 605-10.**

120. **Pathak, I., *et al.*, *Detection of squamous neoplasia by fluorescence imaging comparing porfimer sodium fluorescence to tissue autofluorescence in the hamster cheek-pouch model.* Am J Surg, 1995. 170(5): p. 423-6.**

121. **Onizawa, K., *et al.*, *Fluorescence photography as a diagnostic method for oral cancer.* Cancer Lett, 1996. 108(1): p. 61-6.**

122. **Silberstein, B.R., A. Mayevsky, and B. Chance, *Flying spot studies of brain flavoproteins in the gerbil.* Neurol Res, 1980. 2(1): p. 19-34.**

123. **Nordstrom, R.J., *et al.*, *Identification of cervical intraepithelial neoplasia (CIN) using UV- excited fluorescence and diffuse-reflectance tissue spectroscopy.* Lasers Surg Med, 2001. 29(2): p. 118-27.**

124. **Harries, M.L., *et al.*, *Diagnostic imaging of the larynx: autofluorescence of laryngeal tumours using the helium-cadmium laser.* J Laryngol Otol, 1995. 109(2): p. 108-10.**

125. **Zargi, M., I. Fajdiga, and L. Smid, *Autofluorescence imaging in the diagnosis of laryngeal cancer.* Eur Arch Otorhinolaryngol, 2000. 257(1): p. 17-23.**

126. **Rigacci, L., *et al.*, *Multispectral imaging autofluorescence microscopy for the analysis of lymph-node tissues.* Photochem Photobiol, 2000. 71(6): p. 737-42.**

127. **Kulapaditharom, B., V. Boonkitticharoen, and S. Kunachak, *Fluorescence-guided biopsy in the diagnosis of an unknown primary cancer in patients with metastatic cervical lymph nodes.* Ann Otol Rhinol Laryngol, 1999. 108(7 Pt 1): p. 700-4.**

VII. Tables and Figures

Table 1. Endogenous fluorophores, their excitation and emission maxima, and location in tissue.

Table 2. Exogenous flurophores, their excitation and emission maxima, and representative applications in which they have been used.

Table 3. A comparison of the characteristics of the single-channel flying spot scanner [3], to a multi-channel fluorescence-imaging system developed by Wang et al. [1].

Table 4. Autofluorescence imaging applications organized by tissue site and disease process.

Fig. 1. Fluorescence excitation-emission matrices (EEMs) of (a) normal breast cells (MCF10), and (b) collagen I in the extracellular matrix of an organotypic tissue culture. Each EEM is shown on a color log scale, and each contour corresponds to points of equal fluorescence intensity. The meaningful information is straddled by two sets of Rayleigh scattering lines.

Fig. 2. Low temperature fluorometer, for fluorescence imaging of freeze-trapped tissue blocks. Image adapted from [43].

Fig. 3. Hemotoxylin and eosin (H&E) stained section of a freeze-trapped, normal cervical tissue cross-section and the corresponding autofluorescence images at two excitation-emission wavelength pairs: 440, 525 and 365, 460 nm [44].

Fig. 4. The average fluorescence intensity as a function of tissue depth at (a) 440, 525 nm and (b) 365, 460 nm for normal, inflammatory and severely dysplastic freeze-trapped cervical tissue cross-sections [44].

Fig. 5. Primary components of a generic fluorescence imaging system.

Fig. 6. A schematic of the primary components of the flying spot scanner [3].

Fig. 7. (a) Autofluorescence and reflectance ratio (F/R) images and (b) normalized F/R profiles of the 9L glioma tumor (9 days) and adjacent muscle tissue in the rat flank [3].

Fig. 8. Simulated, normalized fluorescence ratio versus diameter of the illumination-collection aperture for the squamous cell carcinoma (SCC) tissue culture model containing: (a) the SCC layer (without GFP) and (b) the SCC-GFP layer. The legend displays the depth and thickness of the SCC layer corresponding to each profile [8].

Fig. 9. Diameter of the illumination-collection aperture that corresponds to the minimum (for SCC) and maximum (for SCC-GFP) normalized fluorescence ratio (MFR) versus the depth of the SCC layer [8].

Fig. 10. Whole body (A,C,D) and fluorescence microscopic (B) images of liver and skull metastases in live nude mice. (A) A whole body image showing fluorescence from the right and left sides. (B) Fluorescence microscopic image of a cross section, where the level of

development of the tumor corresponds to (A). (C) Ventral image of the liver metastases. (D) Dorsal image of the liver and skull metastases. Image reproduced from [10].

	Endogenous Fluorophores	**Excitation Maxima (nm)**	**Emission Maxima (nm)**	**Primary Tissue Location**
Structural Protein	**Collagen** [21]	325	400, 405	Connective tissue
	Elastin [22, 23]	290, 325	340, 400	Connective tissue
Electron Carrier	**FAD** [24]	450	535	Cells
	NADH [24]	290, 351	440, 460	Cells
Heme-related	**Porphyrins** [25]	400-450	630, 690	Blood
Amino Acid	**Tryptophan** [26, page 15]	280	350	Proteins

Table 1.

	Exogenous Fluorophores	Excitation Maxima (nm)	Emission Maxima (nm)	Representative Applications
Local/systemic introduction	**Aminolevulinic Acid (Protoporphyrin IX)**[95]	375-440	635	Squamous cell carcinoma of the oral cavity in humans [96-98]
				Gastrointestinal cancer in humans [95]
				Bladder cancer in humans [99]
				Squamous cell carcinoma of the rat palatal mucosa [100]
				Malignant gliomas in humans [101]
				Superficial skin cancers in humans [63]
	Carotenohematoporphyrin Derivatives [102]	475-482	627, 695	
	Indocyanine Green and Derivatives [86, 89]	550-780	785-812	Human Serum Albumin and Transferrin labeling in mice [111]
				Monoclonal antibody labeling [89-91]
				Glioma in rats [86]
				Angiography [112]
				Liver biopsy [81]
	Lutetium Texaphyrin[85, 112]	460, 474	740, 732, 750	Squamous cell carcinoma in hamsters [85]
				Ocular fundus angiography and Photodynamic Therapy [112]
	Lanthanide Chelate[113]	270	490, 550, 590	In vivo mice-large intestine [113]
				Disease diagnosis and bone image enhancement [114]
	Ethyl Nile Blue[115]	633	680	Glioma in mice [115]
				Chemically induced mucosal lesions in rats [116]
	Aluminum phthalocyanine disulfonate ($AlPcS_2$) [117]	660	670	Squamous cell carcinoma of the rat palatal mucosa [118]
				Imaging response to Photodynamic Therapy in tumor-bearing mice [117]
	Foscan® (mTHPC) [119]	416, 516, 542, 594, 650	652	Photodynamic Therapy of oral cancer in humans [119]
Genetic introduction	**Luciferase** [103, 104]	NA	548-623	Cancer progression in animal models [9, 13-16]
	Green fluorescent protein (GFP) Mutants [105-109]	360-516	440-583	Lung cancer metastasis in mice [110]
				Whole body imaging in mice [10-12]

Table 2.

Parameters	**Single-Channel System**	**Multi-Channel System**
Power (mW)	15	300
Diameter of illuminated area (mm)	10	40
Power density (mW/mm^2)	2	0.239
Working distance (mm)	60	20
Spatial resolution measured using similar resolution targets (mm)	1.0	0.5
Signal-to-noise (3 x 3 pixel area averaged from 6 frames)	25$\pm$7	32$\pm$5
Frame rate (s)	1	0.033

Table 3.

Tissue site and disease process	Model	In vivo / in vitro	Imaging technique	Reference
Oral cancer	Hamster cheek pouch	In vivo	Endoscopic imaging	[25]
	Hamster cheek pouch	In vivo	Endoscopic (LIFE*) system	[120]
	Hamster, human	In vivo	Fluorescence photography	[121]
Gastrointestinal Tract / Colon cancer	Human	In vitro	Microspectrofluorometry	[41]
	Human	In vivo	Endoscopic imaging	[2], [58], [55]
	Human	In vitro	Confocal microscopy	[39], [4], [42]
	Human	In vitro	Endoscopic imaging	[40]
	Human	In vitro	Microscopy	[38]
Brain tumor	Human	In vitro	Microspectrofluorometry	[37]
	Rat	In vivo	Flying spot scanner	[3], [122]
Cervical cancer	Human	Culture	Microscopy	[5], [6]
	Human	In vivo	Non-endoscopic imaging	[123]
	Human	In vitro	Low temperature imaging	[44]
	Human	In vitro	Microscopy	[32]
Skin melanoma	Human	In vivo	Digital imaging	[62]
	Human	In vitro	Microscopy	[33]
Larynx	Human	In vivo	Endoscopic (LIFE*) system	[124]
	Human	In vivo	Modified Endoscopic (LIFE*) system	[125]
Lung/Bronchus	Human	In vitro	Microscopy	[35]
Breast/Lymph	Human	In vitro	Microscopy	[34]
	Human	In vitro	Multispectral microscopy	[126]
Head and neck	Human	In vivo	Endoscopic (LIFE*) system	[127]
	Human	In vivo	Modified Endoscopic imaging	[57]

* Xillix Technologies Corporation, Richmond, BC, Canada

Table 4.

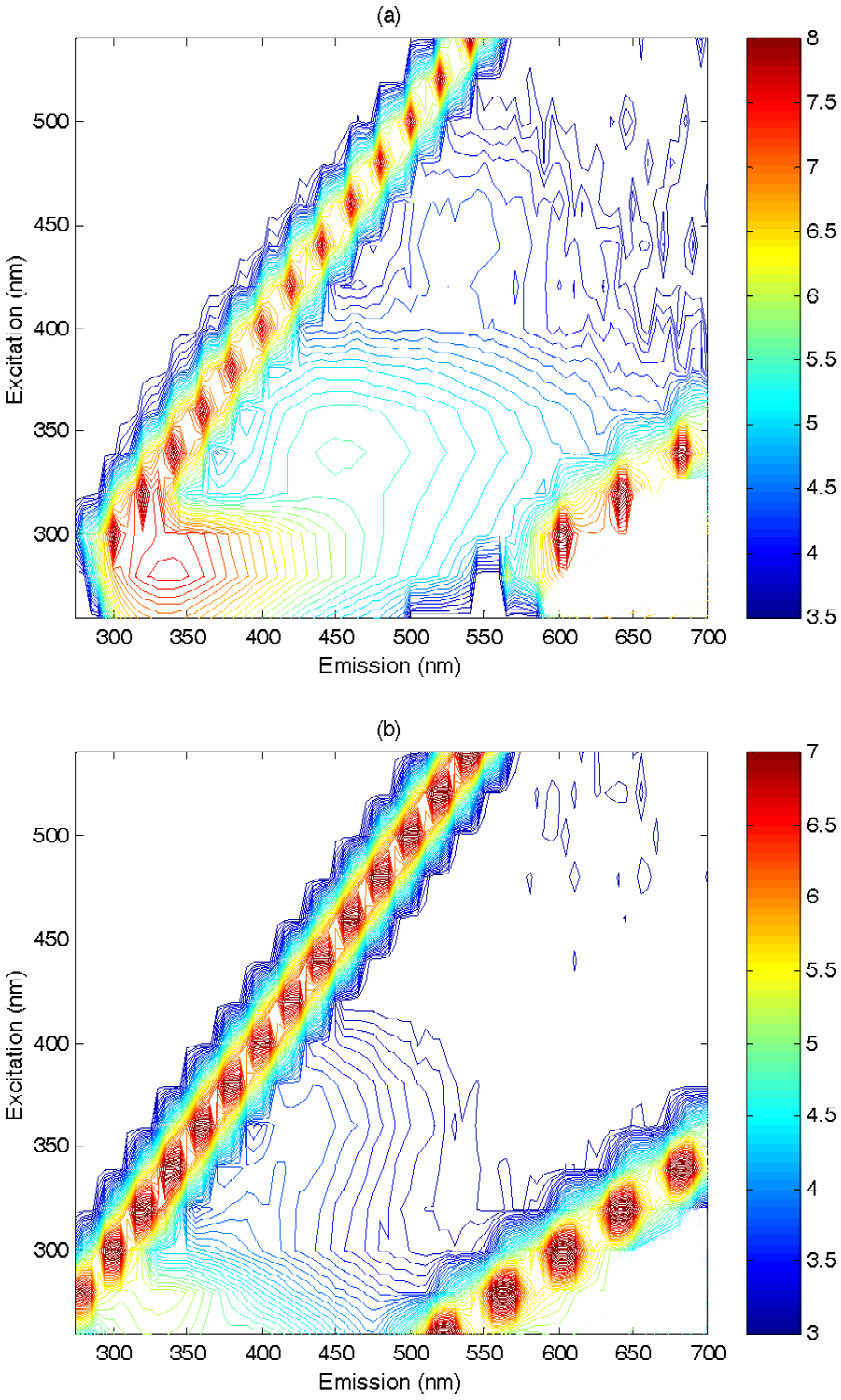
(a)
Excitation (nm)
Emission (nm)
300
350
400
450
500
550
600
650
700
3.5
4
4.5
5
5.5
6
6.5
7
7.5
8
(b)
Excitation (nm)
Emission (nm)
3
3.5
4
4.5
5
5.5
6
6.5
7

Figure 1.

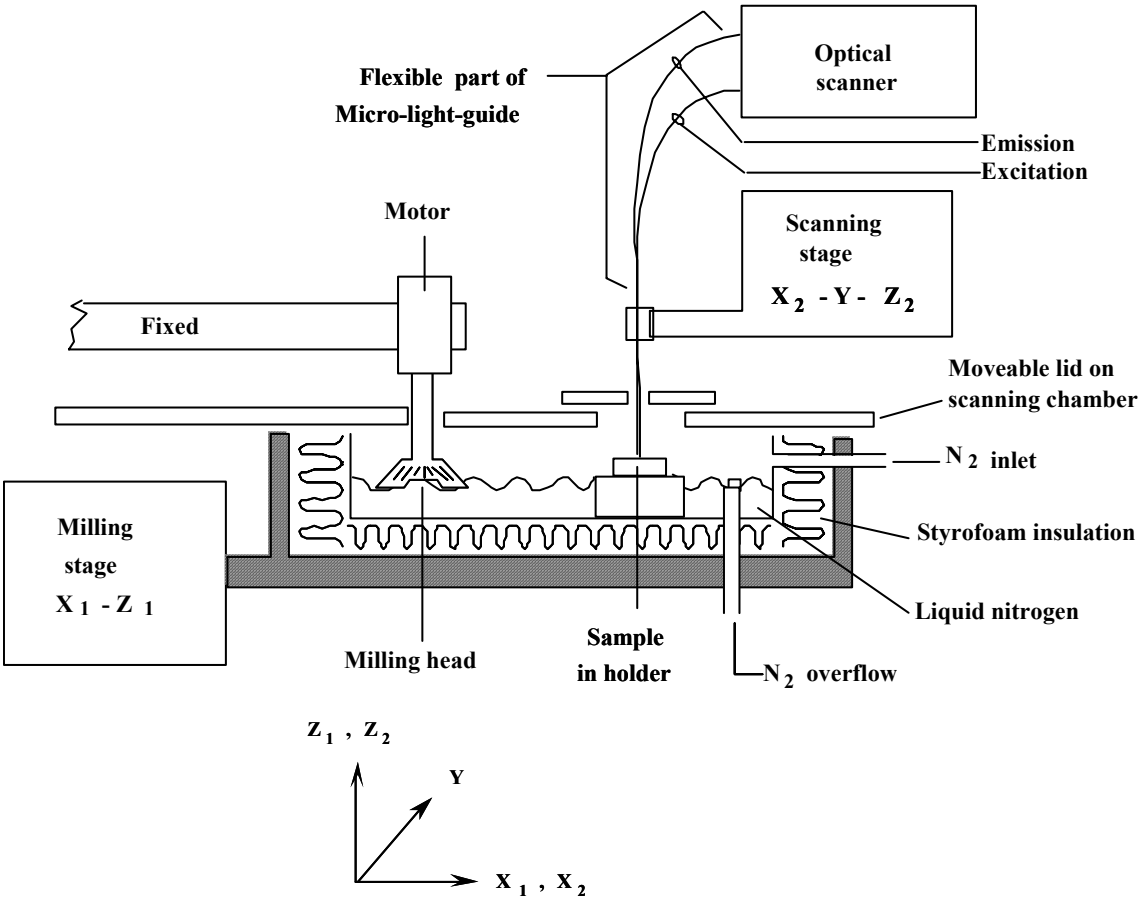
Optical scanner
Flexible part of Micro-light-guide
Emission
Excitation
Motor
Scanning stage
X 2 - Y - Z 2
Fixed
Moveable lid on scanning chamber
N 2 inlet
Milling stage
X 1 - Z 1
Styrofoam insulation
Liquid nitrogen
Milling head
Sample in holder
N 2 overflow
Z 1 , Z 2
Y
X 1 , X 2

Figure 2.

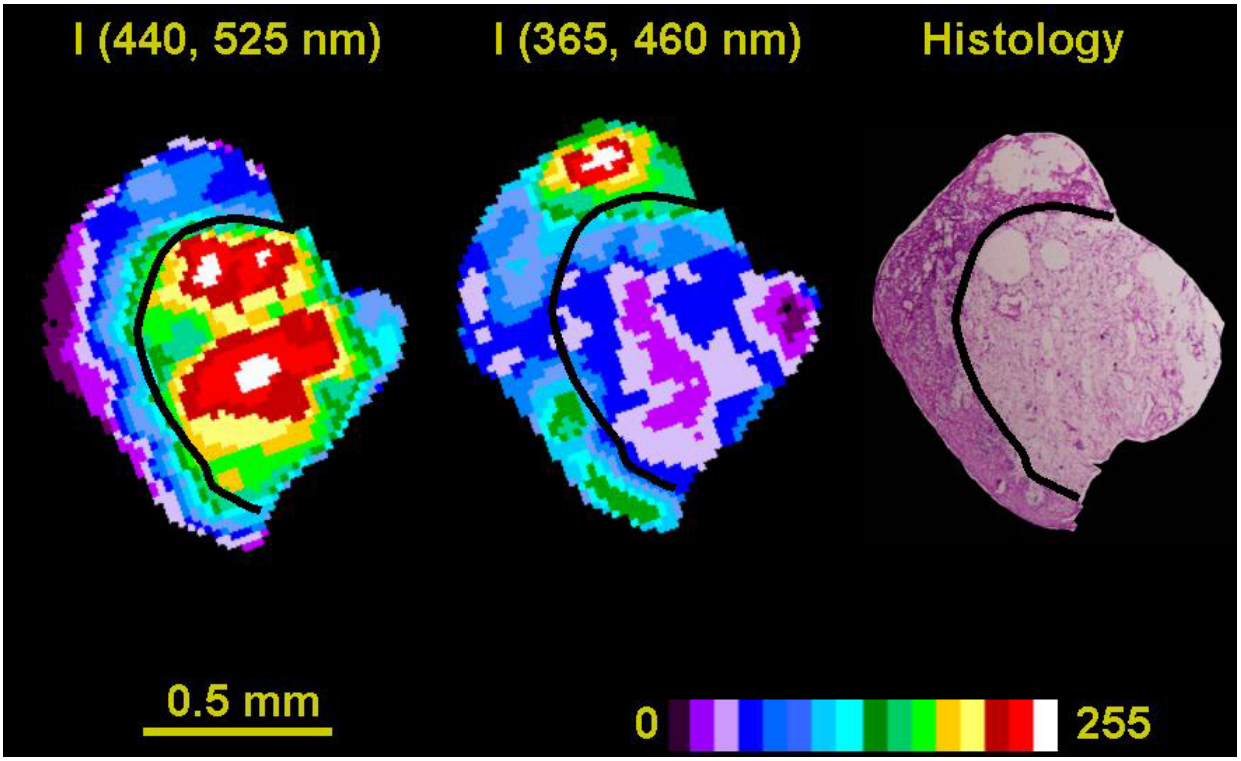

Figure 3.

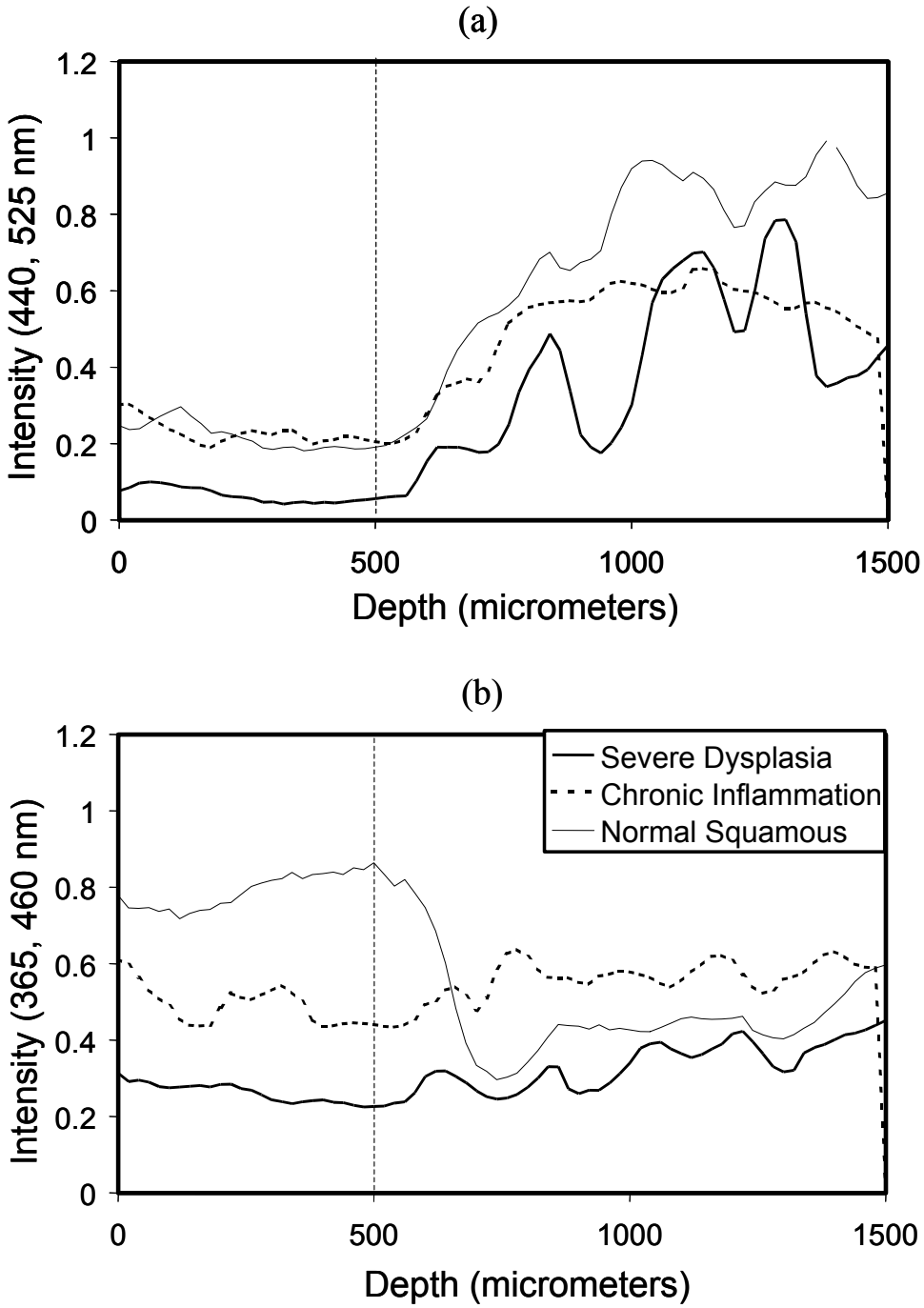
(a)
Intensity (440, 525 nm)
Depth (micrometers)
0
0.2
0.4
0.6
0.8
1
1.2
0
500
1000
1500
(b)
Intensity (365, 460 nm)
Depth (micrometers)
Severe Dysplasia
Chronic Inflammation
Normal Squamous

Figure 4.

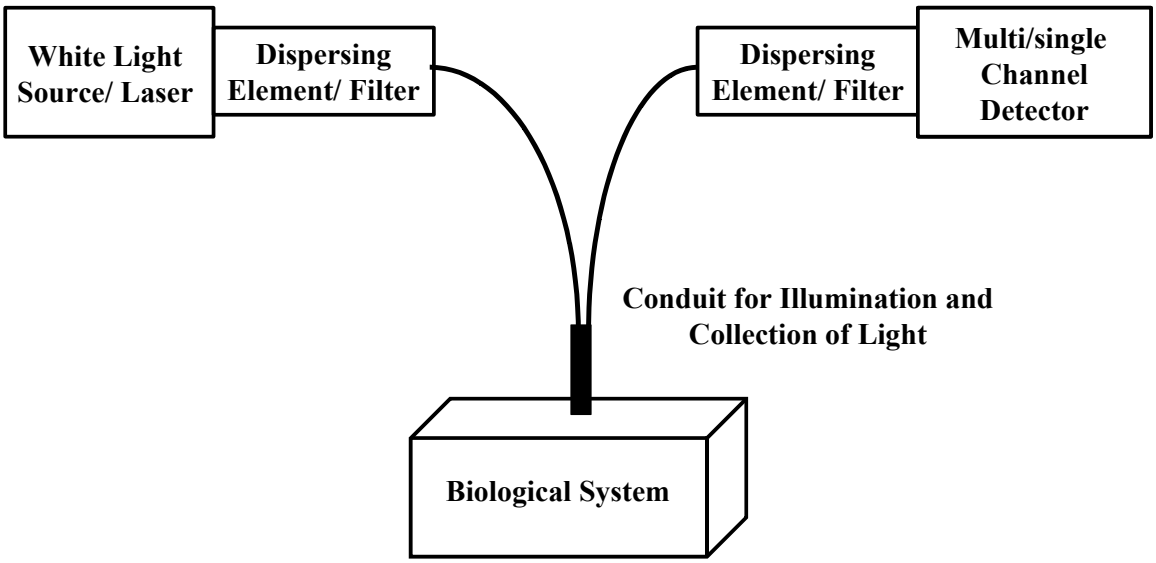
White Light Source/ Laser
Dispersing Element/ Filter
Dispersing Element/ Filter
Multi/single Channel Detector
Conduit for Illumination and Collection of Light
Biological System

Figure 5.

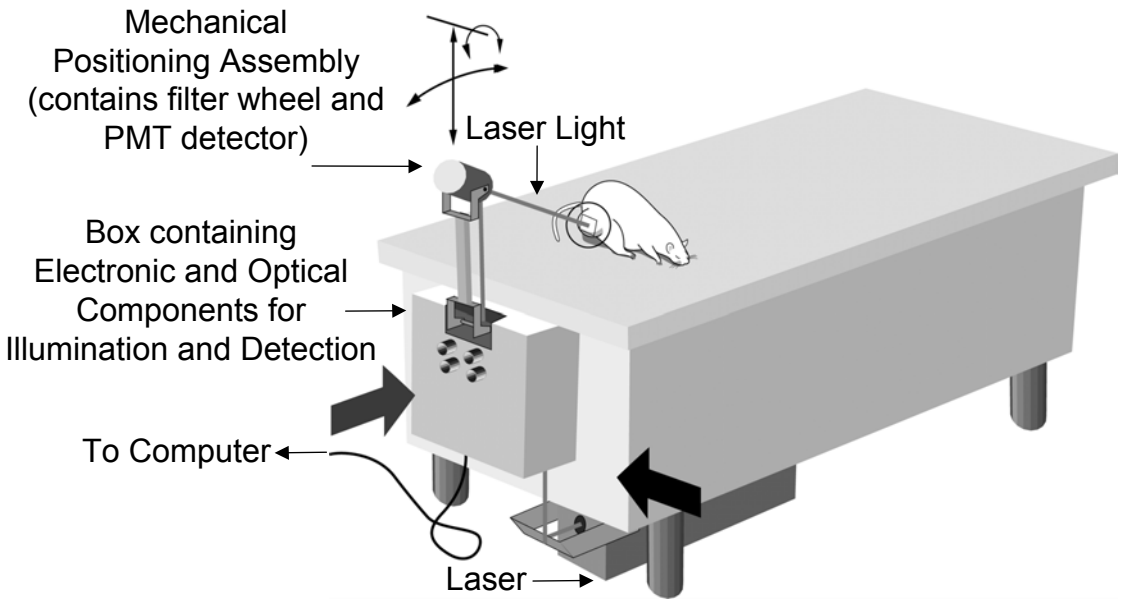
Mechanical
Positioning Assembly
(contains filter wheel and
PMT detector)
Laser Light
Box containing
Electronic and Optical
Components for
Illumination and Detection
To Computer
Laser

Figure 6.

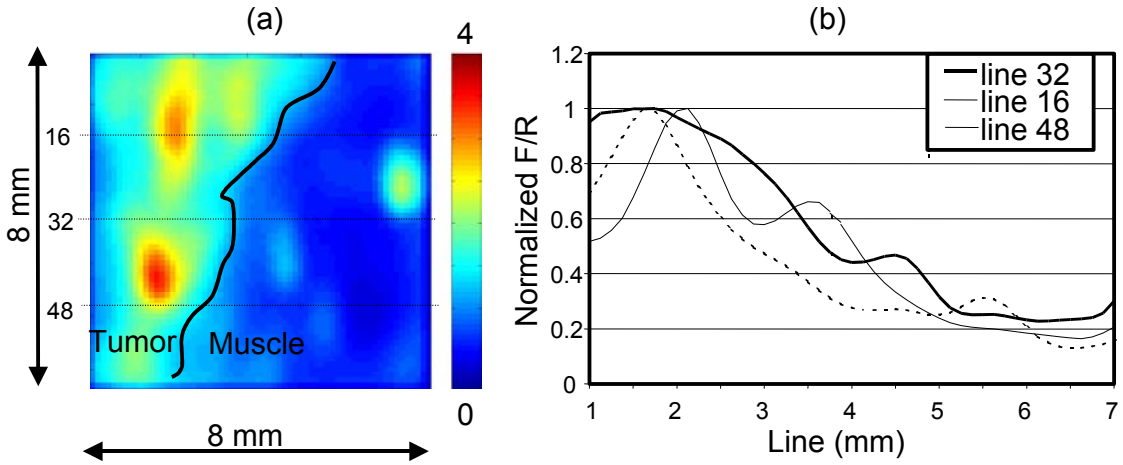
(a)
4
0
16
32
48
8 mm
8 mm
Tumor
Muscle
(b)
Normalized F/R
Line (mm)
line 32
line 16
line 48
1.2
1
0.8
0.6
0.4
0.2
0
1
2
3
4
5
6
7

Figure 7.

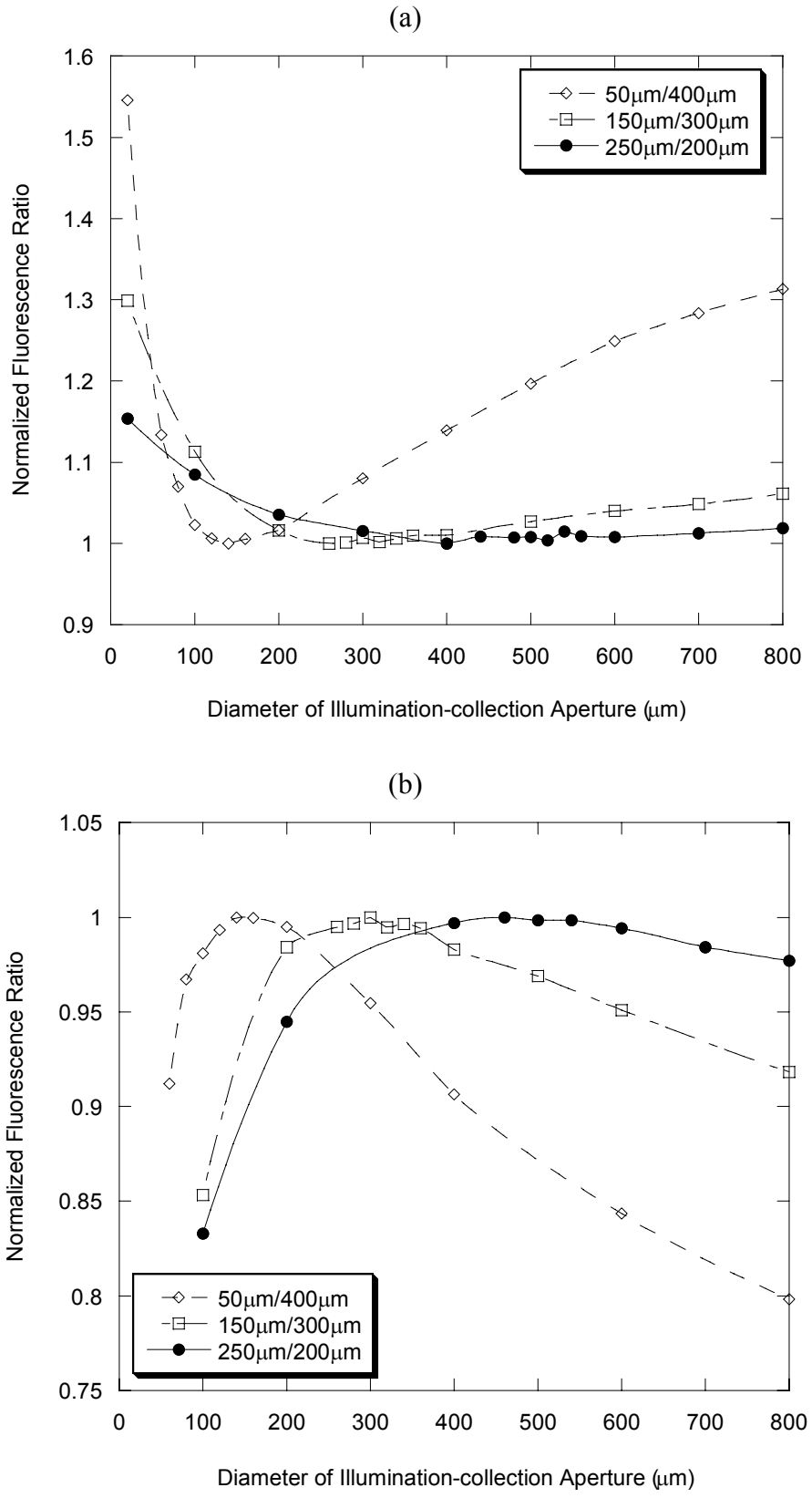
(a)
Normalized Fluorescence Ratio
Diameter of Illumination-collection Aperture (μm)
50μm/400μm
150μm/300μm
250μm/200μm
(b)
Normalized Fluorescence Ratio
Diameter of Illumination-collection Aperture (μm)
50μm/400μm
150μm/300μm
250μm/200μm

Figure 8.

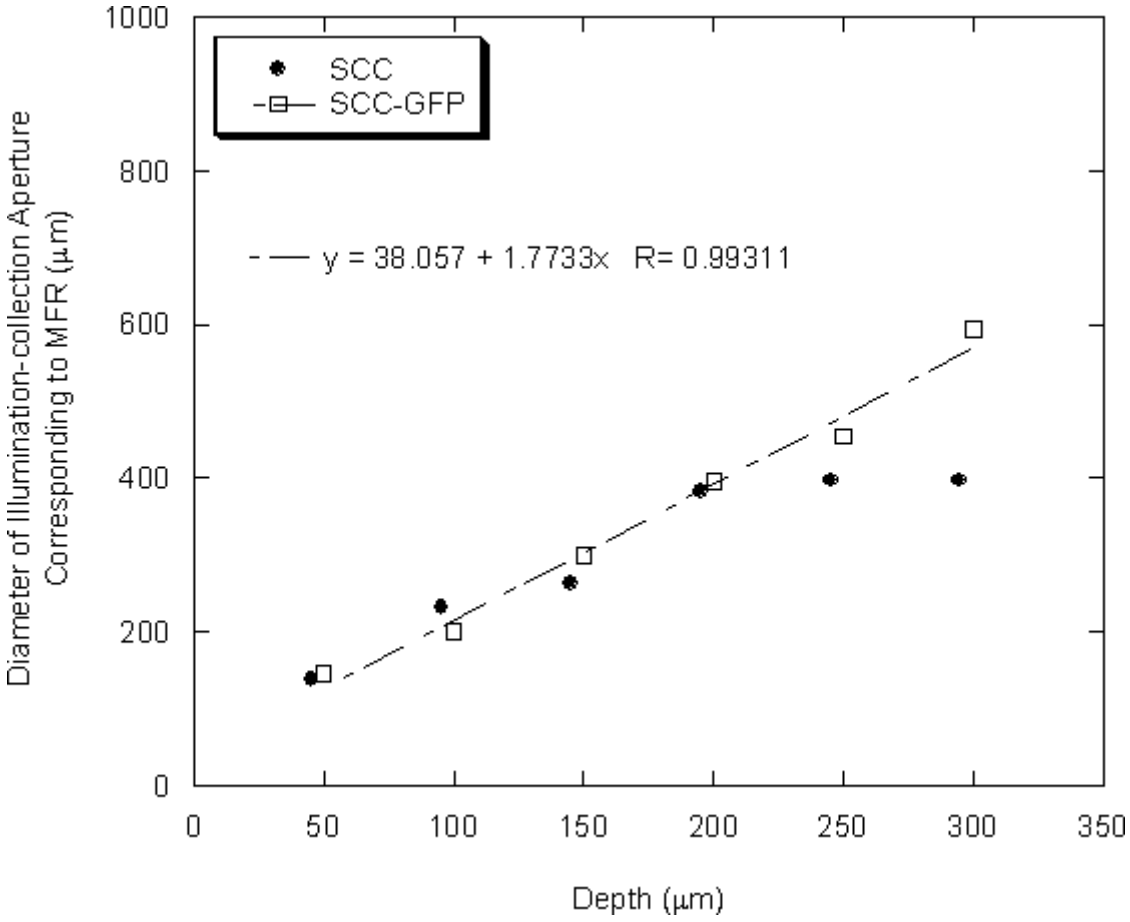
SCC
SCC-GFP
y = 38.057 + 1.7733x R= 0.99311
Diameter of Illumination-collection Aperture Corresponding to MFR (µm)
Depth (µm)
0
200
400
600
800
1000
0
50
100
150
200
250
300
350

Figure 9.

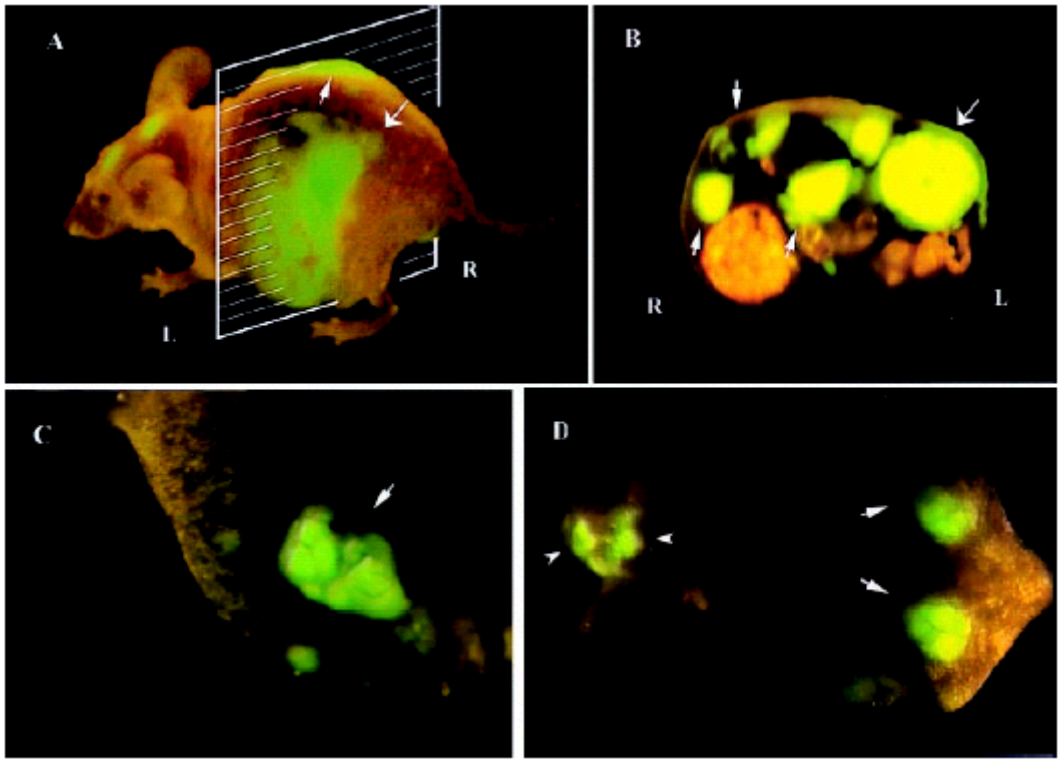

Figure 10.